Plasma assisted Cu-Mn mixed oxide catalysts for trichloroethylene abatement in moist air

Savita Kaliya Perumal Veerapandian, Zhiping Ye, Jean-Marc Giraudon, Nathalie de Geyter, Rino Morent, Jean-Francois Lamonier

Plasma assisted Cu-Mn mixed oxide catalysts for trichloroethylene abatement in moist air

Savita Kaliya Perumal Veerapandian[a], Zhiping Ye[a,b], Jean-Marc Giraudon[b], Nathalie De Geyter[a], Rino Morent[a], Jean-Francois Lamonier[b*]

[a]*Ghent University, Faculty of Engineering and Architecture, Department of Applied Physics, Research Unit Plasma Technology, Sint-Pietersnieuwstraat 41 B4, 9000 Ghent, Belgium*

[b]*Univ. Lille, CNRS, Centrale Lille, ENSCL, Univ. Artois, UMR 8181 - UCCS - Unité de Catalyse et Chimie du Solide, F-59000 Lille, France*

*Corresponding author: jean-francois.lamonier@univ-lille.fr

Abstract

The removal of dilute trichloroethylene (TCE) in moist air by post-plasma catalysis (PPC) using Cu-Mn mixed oxides heated at 150°C was investigated. Cu-Mn mixed oxides were prepared by redox- and co-precipitation method. In comparison to the catalytic oxidation and non-thermal plasma (NTP) process, PPC was found to be the best process to convert TCE into CO_2, in particular when Cu-Mn oxide was synthetized by redox precipitation method. The highest TCE conversion efficiency of more than 80% was obtained at the energy density of 60 $J.L^{-1}$ using the catalyst prepared by redox-precipitation process in PPC configuration. The performance of Cu-Mn oxide prepared by redox-precipitation method does not show increase in TCE conversion with energy density which is attributed to the changes on the catalyst surface (such as reduction in S_{BET}, chlorine poisoning and Mn enrichment). Although, Cu-Mn oxide prepared by co-precipitation method showed a lower TCE conversion, it exhibited a better stability in the PPC process for TCE abatement.

Keywords: Post Plasma-Catalysis; TCE abatement; Cu-Mn mixed oxides; Non-thermal plasma

1. Introduction

Volatile organic compounds (VOCs) form a major source of pollution in indoor and outdoor air. Due to their adverse impacts on environmental and human health [1], VOC removal from waste gas streams with high efficiency at low cost is an issue of major concern. In recent years, various techniques such as adsorption, thermal incineration, catalytic oxidation, membrane separation [2–5], etc., have been used for VOC removal. However, the conventional techniques are not energy efficient for the removal of diluted VOCs (< 1000 ppmv) from the waste gas [6]. Non-thermal plasma (NTP) has been identified as a cost and energy effective method for the removal of diluted VOCs [7–10]. In NTP technology, the input electrical energy is selectively transfer to electrons which generate free radicals enabling the decomposition of the pollutants. However, the major drawback of NTP technique for the removal of VOCs is low selectivity inducing formation of toxic by-products such as NO_x, O_3 and possible other hazardous VOCs. In order to overcome the drawbacks of individual techniques, the combination of two techniques have been proposed in order to take advantages of each technique alone. Among the different possibilities, the hybrid technique of plasma-catalysis by combining non-thermal plasma (NTP) and catalytic oxidation has been widely investigated for the decomposition of VOCs from waste gas [11,12]. For plasma-catalysis technique, the catalyst can be placed either downstream of the plasma reactor (post plasma-catalysis-PPC) [13,14] or in the plasma discharge region (in plasma-catalysis-IPC) [15–17].

In special case of PPC configuration, the choice of the catalyst has a great influence on the performance of the hybrid system, all other operating parameters of the process considered as similar. In order to get

a higher efficiency of the hybrid system for TCE abatement, a set of design criteria of the catalyst has been previously outlined such as high ozone decomposition ability, oxygen mobility, high CO_2 selectivity in moist air coupled with a good resistance to chlorine. The catalyst has to be also cost-effective and benign to the environment. Taking into account these criteria, the performance of MnO_2 catalysts in PPC has been particularly investigated due to its high capacities for ozone decomposition to supply active oxygen species enabling the decomposition of the plasma generated hazardous by-products more prone to oxidation than the parent TCE [18]. With that respect, the performances of various Mn based oxide catalysts as single oxides [19], mixed oxides [20–23] or doped with traces of Pd [14] or with Fe [24] have been investigated so far by our teams in the case of TCE oxidation in dry and/or moist air using a multi-pin-to-plate NTP reactor working in DC negative corona discharge [25]. Furthermore, some studies have stressed the beneficial role of using manganese containing binary metal oxides for the total oxidation of VOCs. On purpose Cu-Mn mixed oxide catalysts (commercially known as Hopcalite) are of prime importance due to their remarkable abilities for CO oxidation at low temperature and O_3 decomposition [26–30]. The CO removal ability of Cu-Mn mixed oxide catalysts has been reported elsewhere to be related to the formation of a $CuMn_2O_4$ spinel phase [28]. It is expected that the catalytic performance of this promising catalyst towards TCE total oxidation could be closely dependent on the method of preparation. In this work, the Cu-Mn mixed oxide catalysts have been prepared by a conventional method (co-precipitation [31]) and by an alternative route (redox-precipitation [32]). In comparison to catalytic oxidation of chlorinated VOCs using Cu-Mn mixed oxide catalysts [30,33,34], the works carried out in plasma catalysis using Cu-Mn mixed oxide catalysts are rather scarce.

In this study, the effect of two copper manganese oxide catalysts on the performances of TCE total oxidation in PPC has been investigated in moist air (Relative Humidity (RH) =15%) at a catalytic reactor temperature of 150˚C as a function of energy density (ED) delivered by a ten pin-to-plate NTP reactor using a DC negative corona discharge. For better comparison, the TCE abatement has been also investigated using NTP alone at 25 ˚C and over the catalyst alone from 100 to 300˚C for every 50˚C. The performances of each configuration were evaluated in terms of TCE conversion, CO_2 yield, CO_x yield and formation of gaseous by-products. The fresh and used catalysts were characterized in order to obtain some correlations between physico-chemical properties and performances in TCE abatement.

2. Experimental section

2.1 Catalyst preparation

The detailed description of the catalyst preparation methods was given elsewhere [35]. The copper manganese oxide catalysts were prepared by redox- and co- precipitation methods and were labelled $CuMnO_x$-R3 and $CuMn_2O_4$-P4, respectively. In brief, $CuMnO_x$-R3 was prepared through reaction of copper(II) nitrate with manganese(II) acetate as reductant and potassium permanganate as oxidant. The powder obtained from the resultant suspension was dried overnight at 100 °C and calcined in dry air at 300˚C for 2 hours. $CuMn_2O_4$-P4 was prepared by addition of a tetramethylammonium hydroxide (TMAH) aqueous solution to an aqueous solution of copper(II) and manganese(II). The resulting suspension was allowed to maturate for 2 hours. After filtration and drying, the obtained powder was calcined in dry air at 400˚C for 5 hours.

2.2 Catalyst characterization

Elemental analyses of Cu and Mn for the calcined catalysts samples were determined at REALCAT platform (University of Lille) by inductively coupled plasma-optical emission spectroscopy (ICP-OES) using an Agilent Technologies 700 Series spectrometer. The samples were treated with *aqua regia* before analysis.

N_2 physisorption measurements were carried out at liquid nitrogen temperature (-196˚C) using a Micromeritics Flow Sorb III apparatus. The samples were degassed at 150˚C for a few hours in nitrogen prior measurements. The specific surface areas were calculated using the BET method; the pore size distribution was determined using the BJH method and the total pore volume (V_p) was estimated from the total amount of N_2 adsorbed to a relative pressure of 0.99.

X-ray photoelectron spectroscopy (XPS) was carried out using a KRATOS, AXIS Ultra Spectrometer with a Al K_α radiation source ($h\nu$ = 1486.6 eV) and a hemispherical analyzer with constant ΔE/E. The binding energies (BEs) were corrected from the C 1s carbon peak located at 284.8 eV as an internal standard. The processing and curve-fitting of the high resolution spectra were performed using CasaXPS software. The detailed explanation about the determination of the XPS Mn average oxidation state (Mn AOS) from the Mn 3s core-level spectrum as well as the extraction of the Cu 2p component and associated satellites corrected from the Mn LMM_b Auger contribution were given elsewhere [35]. For the used samples, the simulation of the Cl 2p core level was carried out considering equal FWHM for the two Cl $2p_{3/2}$ and Cl $2p_{1/2}$ spin orbit peaks with a separation of 1.6 eV.

2.3 TCE Abatement

The schematic of the experimental set-up used for all experiments of TCE abatement (non-thermal plasma (NTP), catalytic oxidation (C) and post-plasma catalysis (PPC)) including a flue gas generation system, a plasma-catalysis reactor and instrumentation for the analysis of exhaust gas was already shown elsewhere [24]. Trichloroethylene (TCE, 99.99% purity, ACROS) was evaporated by bubbling moist air (RH=15%) into a saturator and introduced into the plasma reactor after diluting with air. The total flow rate and TCE concentration were maintained at 0.5 $L.min^{-1}$ and ~ 300 ppmv (6.15 $\mu mol.min^{-1}$), respectively, using mass flow controllers (MFC, El-Flow, Bronkhorst). A 10-pin-to-plate plasma reactor configuration was used working in a negative DC corona discharge. A detailed description of the geometry of the plasma reactor and the electrical measurements were given somewhere else [36–38]. 0.5 g of catalyst diluted in 3 g of SiC (EMB 45053 Prolabo, 0.105 mm) placed in a quartz reactor was calcined for 4 hours in dry air (0.2 $L.min^{-1}$) at 300˚C.

The performances for TCE abatement in terms of TCE conversion, CO_2 and CO_x yields (x = 1 and 2) of the three processes *i.e.* NTP, C and PPC were separately assessed using the same set-up described above. The associated values of the operating parameters for these three distinct experiments were summed-up in **Table 1**. The gaseous products at the exit of the catalytic reactor were analyzed using a FT-IR spectrometer (Bruker, Vertex 70) equipped with a gas cell of 20 cm optical path length. The FT-IR spectra averaged over 10 samples were obtained with the resolution of 4 cm^{-1}. Ozone formation was determined using a UV absorption based ozone detector (Teledyne, model 465M). The catalysts after catalysis alone and PPC were named with the same coding at which the suffix C and PPC were added, respectively.

The following parameters were used to evaluate the efficiency of the process:

The TCE abatement (conversion) efficiency was calculated from:

$$\text{TCE abatement}\ (\%) = \frac{[\text{TCE}]_{\text{in}} - [\text{TCE}]_{\text{out}}}{[\text{TCE}]_{\text{in}}} \times 100 \quad (1)$$

where $[\text{TCE}]_{\text{in}}$ and $[\text{TCE}]_{\text{out}}$ were the inlet and outlet TCE concentrations, respectively.

The CO_2, CO and CO_x yields were calculated as follows:

$$Y_{CO_2}(\%) = \frac{[\text{CO}_2]_{\text{out}}}{2 \times [\text{TCE}]_{\text{in}}} \times 100 \quad (2)$$

$$Y_{CO}\ (\%) = \frac{[\mathrm{CO}]_{\mathrm{out}}}{2\times[\mathrm{TCE}]_{\mathrm{in}}} \times 100 \quad (3)$$

$$Y_{CO_x}\ (\%) = Y_{CO_2}\ (\%) + Y_{CO}\ (\%) \quad (4)$$

where $[\mathrm{CO_2}]_{\mathrm{out}}$ and $[\mathrm{CO}]_{\mathrm{out}}$ were the outlet concentrations of CO_2 and CO, respectively.

Table 1. Experimental conditions used for NTP alone, catalytic oxidation alone and PPC experiments

Non thermal plasma alone (NTP)	
Air source	Dry air cylinder
Flow rate	0.5 $L.min^{-1}$
Relative Humidity (20 °C)	15 %
Initial TCE concentration	~ 300 ppmv (6.15 $\mu mol.min^{-1}$)
Energy density	60 - 120 $J.L^{-1}$ (step of 30 $J.L^{-1}$; 10 minutes for every ED)
Catalytic oxidation (C)	
Air source	Dry air cylinder
Activation conditions	200 $mL.min^{-1}$, 300 °C for 4 h
Catalyst Temperature	100-300 °C (at intervals of 50 °C; 60 minutes at a given temperature)
Heating rate	2 $°C.min^{-1}$
Flow rate	0.5 $L.min^{-1}$
Gas hourly space velocity (GHSV)	60,000 $mL.g^{-1}.h^{-1}$
Relative Humidity (20 °C)	15 %
Initial TCE concentration	~ 300 ppmv (6.15 $\mu mol.min^{-1}$)
Catalyst	0.5 g /3 g SiC
Post Plasma Catalysis (PPC)	
Air source	Dry air cylinder
Activation conditions	200 $mL.min^{-1}$, 300 °C for 4 h
Flow rate	0.5 $L.min^{-1}$
Relative Humidity (20 °C)	15 %
Initial TCE concentration	~ 300 ppmv (6.15 $\mu mol.min^{-1}$)
Energy density	60 - 120 $J.L^{-1}$ (step of 30 $J.L^{-1}$; 60 minutes for every ED)
Catalyst Temperature	150 ˚C
Catalyst	0.5 g /3 g SiC

3. Results and discussion

3.1. TCE Abatement

3.1.1 Non Thermal Plasma

Figure 1 shows the TCE abatement and the concentration of ozone produced during the NTP treatment as a function of ED. The TCE removal efficiency linearly increases with ED. This result can be explained by the formation of more energetic electrons which produce more reactive species enable to react with TCE. The highest TCE removal efficiency is 56 % for an ED of 120 J.L^{-1}. Furthermore, an increase of ED also leads to an increase in the production of ozone which amounts to 200 ppmv at 120 J.L^{-1}. The oxygen atoms produced in the discharge, whose production increases with the energy of electrons, form ozone by three body collisions implying dioxygen molecules [39,40].

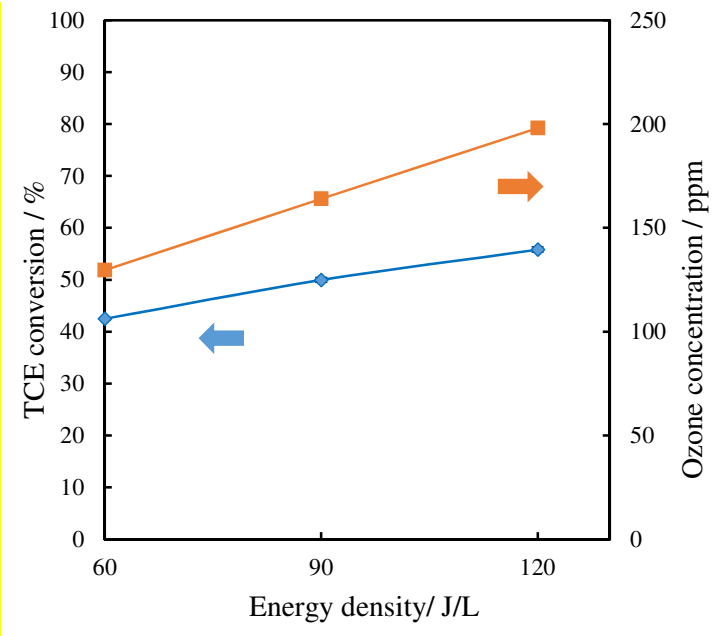

Figure 1. TCE conversion with error and ozone concentration as a function of ED in NTP process

Figure 2 shows the CO and CO_2 yields obtained during the NTP experiments as a function of ED. Although the CO and CO_2 yields increase with ED, it is found a poor mineralization of TCE into CO_x as the highest CO_x yield is 13% for ED of 120 J.L^{-1}. This low CO_x yield in NTP experiments has been previously explained by the formation of hazardous polychlorinated organic by-products such as phosgene ($COCl_2$), dichloroacetylchloride ($CHCl_2$–COCl = DCAC) and trichloroacetaldehyde (Cl_3C-CHO = TCAD) [36].

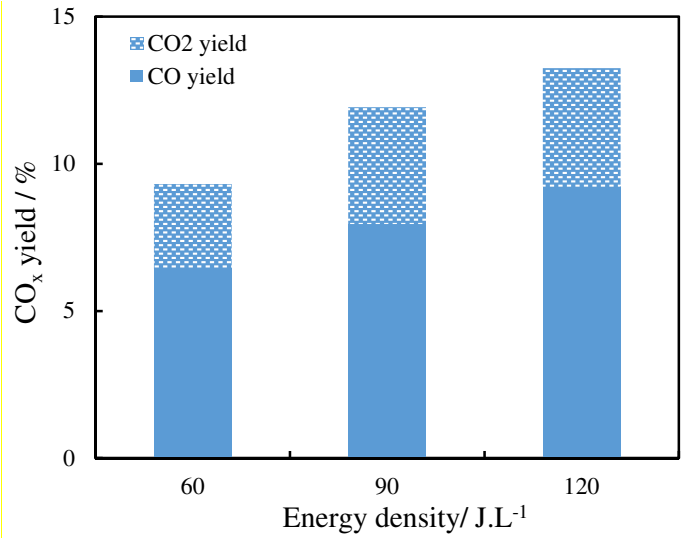

Figure 2. CO and CO_2 yields as a function of ED in NTP process

3.1.2 Catalytic oxidation

Figure 3a shows the TCE abatement in moist air obtained during the catalytic TCE oxidation reaction at different temperatures ranging from 100 to 300 ˚C after 50 minutes for 10 minutes at the temperature under study over the $CuMnO_x$-R3 and $CuMn_2O_4$-P4 catalysts. The TCE removal is significant at 250 °C over $CuMn_2O_4$-P4 amounting to 19 % and 50 % at 300 °C. A significant improvement in catalytic activity is observed when $CuMnO_x$-R3 is used since 45 % and 94 % of TCE were removed at 250°C and 300°C, respectively.

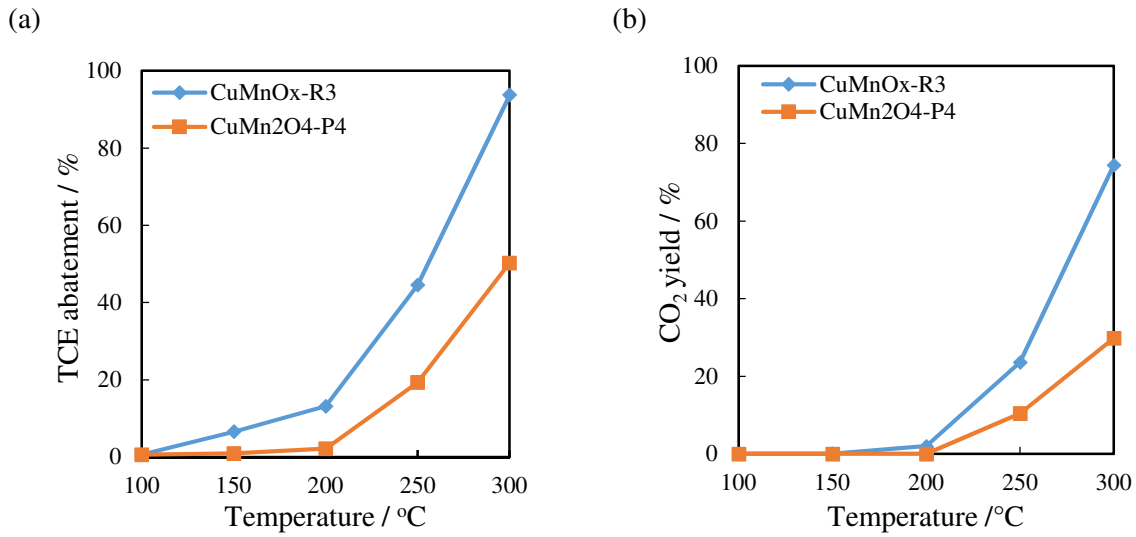

Figure 3. (a) TCE abatement and (b) CO_2 yield obtained through the TCE oxidation reaction over $CuMn_2O_4$-P4 and $CuMnO_x$-R3 catalysts at different temperatures

It is found for both catalysts CO_2 as the main gaseous oxidation C1 product whose characteristic FT-IR bands are shown in **Figure 4**. The detection of CO as trace amount can be explained from the well-known ability of copper-manganese oxide to oxidize easily CO into CO_2 even in humid conditions [27]. **Figure 3b** shows the corresponding CO_2 yields. The difference between TCE abatement (**Figure 3a**) and CO_2 yield (**Figure 3b**) for $CuMnO_x$-R3 can be explained at low temperature (≤ 200 °C) by the presence of some chemisorbed TCE related oxidized species bound to the surface in accordance with a higher S_{BET} as shown below.

Until 250 °C, the catalyst $CuMn_2O_4$-P4 is 100% selective into CO_2. By opposition at 300 °C, the formation of C_2Cl_4 as by-product was observed by FT-IR spectroscopy. It is found in **Figure 5** the characteristic vibration bands of perchloroethylene (PCE) at 916 cm^{-1} at 804 and 781 cm^{-1} [41]. Similarly, over $CuMnO_x$-R3 oxide, the TCE conversion increases as well as the CO_2 yield with temperature. It is noticeable, however, C_2Cl_4 has already been detected at 250°C (**Figure 5**).

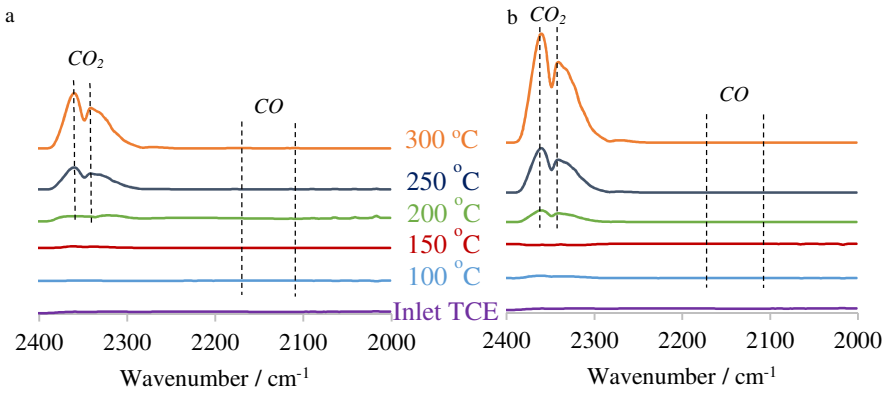

Figure 4. FT-IR spectra in the wavenumber range 2400 –2000 cm^{-1} of inlet TCE polluted air stream and outlet stream after catalytic oxidation (Catalysts: (a) $CuMn_2O_4$-P4 and (b) $CuMnO_x$-R3; Temperature: 100-300°C)

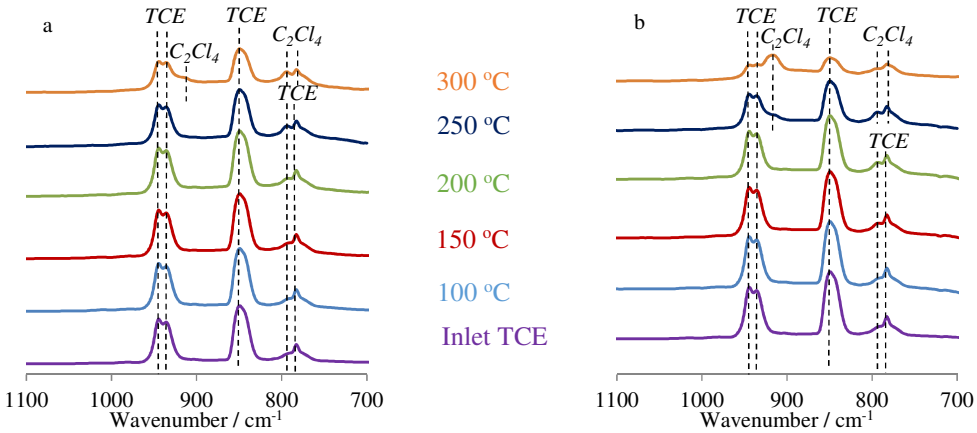

Figure 5. FT-IR spectra in the wavenumber range 1100 – 700 cm^{-1} of inlet TCE polluted air stream and outlet stream after catalytic oxidation (Catalysts: (a) $CuMn_2O_4$-P4 and (b) $CuMnO_x$-R3; Temperature: 100-300°C)

The redox behavior of the catalysts has been previously investigated from H_2-TPR experiments [35]. It is found that the amount of hydrogen consumed at low temperature range (150-250°C) is much more important in $CuMnO_x$-R3 sample than that in $CuMn_2O_4$-P4 sample. This higher amount of reducible oxygen species can explain the presence of some chemisorbed TCE related oxidized species at the surface of $CuMnO_x$-R3.

Table 2 summarizes the textural properties of the fresh and used catalysts. The relative higher external surface obtained for the fresh $CuMnO_x$-R3 in comparison to that of $CuMn_2O_4$-P4 is in line with its mean crystallite size [35]. This indicates a better dispersion of the Cu-Mn oxide entities allowing a better amount of chemisorbed species at a low temperature range as previously noted. After the catalysis experiment, the specific surface area of both catalysts decreases significantly and the specific surface area of $CuMnO_x$-R3 sample remains the highest despite that its relative decrease (~ 61 %) is more pronounced than that for $CuMn_2O_4$-P4 sample (~ 35 %).

Table 2. Textural properties and element contents of fresh and used catalysts

Sample	S_{BET} ($m^2.g^{-1}$)	Vp[a] ($m^3.g^{-1}$)	Dp[b] (nm)	Mn (wt%)	Cu (wt%)	Mn/Cu[c]
$CuMn_2O_4$-P4	48	0.30	21.0	47.05	30.59	1.8
$CuMn_2O_4$-P4-C	31	0.32	33.5	-	-	-
$CuMn_2O_4$-P4-PPC	30	0.29	39.3	46.87	28.52	1.9
$CuMnO_x$-R3	166	0.30	10.0	48.41	11.66	4.8
$CuMnO_x$-R3-C	63	0.46	28.0	-	-	-
$CuMnO_x$-R3-PPC	68	0.41	21.1	45.13	9.95	5.2

[a] BJH Desorption cumulative volume of pores; [b] BJH Desorption average pore diameter; [c] Atomic ratio

The catalytic properties (T_{50}, stability, by-products formation) of some catalysts obtained in the total oxidation of TCE (various experimental conditions) are listed in **Table 3**. This overview highlights the good catalytic activity of $CuMnO_x$-R3 in TCE removal in moist air. Indeed the temperature at which 50 % of TCE is converted (T_{50}) is around 260°C. Li et al. [42] obtained a lower T_{50} value (< 100 °C) but the experiments have been carried out with a four time lower GHSV.

Table 3. Overview of TCE oxidation over different catalysts

Catalyst	Feed (RH in %)	TCE (ppmv)	GHSV ($mL.g^{-1}.h^{-1}$)	T_{50} (°C)	Stability	Products	Ref.
$CuMnO_x$-R3	Humid air (15)	300 (6.15)*	60,000	255[a] (246)[b]	-	C_2Cl_4 (250 to 300 °C), CO, CO_2,	This work
$CuMn_2O_4$-P4	Humid air (15)	300 (6.15)*	60,000	300[a] (244)[b]	-	C_2Cl_4 (300 °C), CO, CO_2	
4.7 wt% Co-Al	Dry air	1000 (16.39)*	35,000	280[a] (400)[b]	~ 50% TCE removal after 70 h at 300 °C	HCl, Cl_2, CO_2, C_2Cl_4	[43]
H–Y zeolite	Humid air (60)	1000 (20.49)*	35,000	~480[a]	-	CO, CO_2, HCl, Cl_2, C_2Cl_4	[44]
1.88 wt% Fe-ZSM-5	Dry air	1000 (18.44)*	32,000	~ 380[a]	100 % TCE removal after 16.7 h at 500 °C	-	[45]

Cu- β zeolite	Dry air	1000 (16.39)*	35,000	310[a] (> 550)[b]	~ 45% TCE removal after 70 h at 300°C	CO, CO_2, HCl, Cl_2, C_2Cl_4	[46]
H-ZSM-5	Dry air	1000 (20.49)*	50,000	510[a]	~ 38 % to ~10% TCE removal after 13.8 h at 500°C	-	[47]
0.42 wt% Pd/ Al_2O_3	Dry air	1000 (20.49)*	35,000	400[a] (~ 425)[b]	-	CO, CO_2, HCl Cl_2, C_2Cl_4	[48]
$CoCr_2O_4$	Humid air (60)	1500 (20.49)*	48,000	~290[a]	-	-	[49]
Pt/Al_2O_3 (Johnson Matthey)	Humid air (1 vol.% H_2O)	200	10,000 h^{-1}	~ 270[a]	-	CO_2, HCl, H_2O, $CHCl_3$, CCl_4, C_2Cl_4	[50]
0.15 wt% Pt/ Al_2O_3 (Chemical Plant OSWIJZCIM)	Dry air	746	10,000 h^{-1}	~ 280[a]	-	-	[51]
Ce-Mn oxides (Mn/(Mn + Ce) = 0.21)	Dry air	1000 (2.05)*	15,000 h^{-1}	87[a]	100 % TCE removal after 20h at 200°C	CO_2, H_2O, HCl, Cl_2	[42]

* molar flow rate in µmol.min^{-1}

[a] from total conversion of TCE [b] from TCE converted to CO_2

3.1.3 Post plasma catalysis

Figure 6 shows the TCE conversion as a function of ED (60 - 120 J.L^{-1}) over the two catalysts ($CuMnO_x$-R3 and $CuMn_2O_4$-P4). For comparison, the TCE conversion data for NTP alone and catalysis alone (150 °C) are also reported. The efficiency in terms of TCE abatement of the 3 processes decreases owing to the following sequence: PPC > NTP > C.

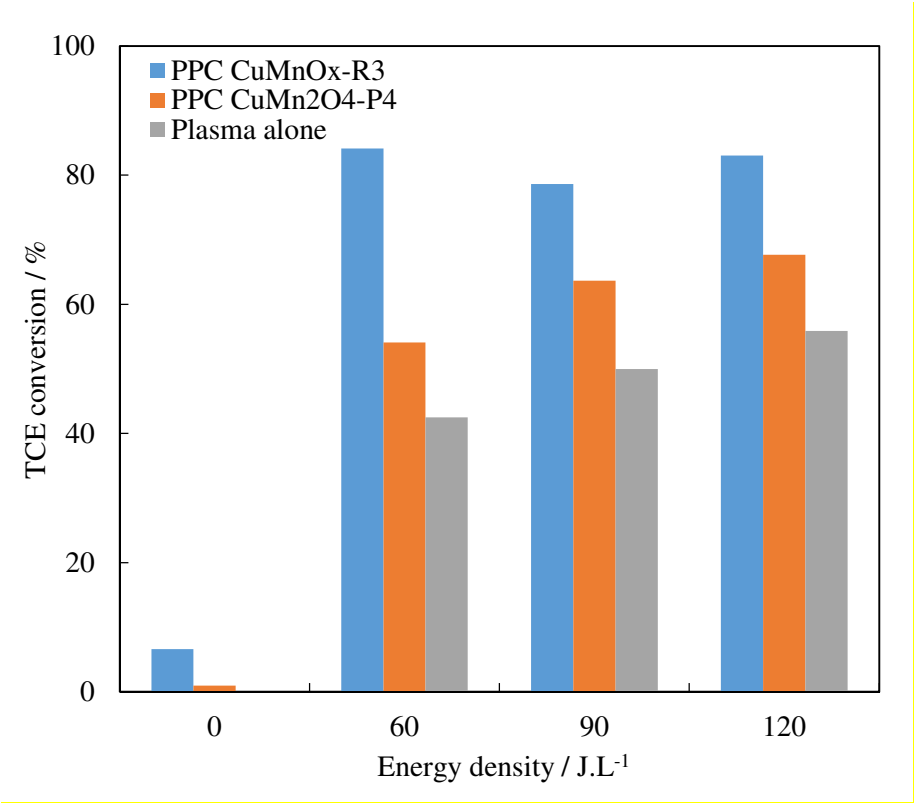

Figure 6. TCE conversion for catalytic oxidation (ED = 0 J.L^{-1}; catalyst temperature = 150 ˚C), NTP (ED = 60, 90 and 120 J.L^{-1}) and post-plasma catalysis (ED = 60, 90 and 120 J.L^{-1}; catalyst temperature = 150 ˚C) experiments

Among the 2 PPC configurations that with $CuMnO_x$-R3 downstream of the NTP outperforms the one with $CuMn_2O_4$-P4 irrespective of the applied ED. However, as the TCE abatement increases with ED for PPC-$CuMn_2O_4$-P4 no improvement was noticeable for PPC-$CuMnO_x$-R3 suggesting a possible degradation of the catalyst in the course of the reaction. Such a degradation might be partly related to a decrease of the S_{BET} of the catalyst for $CuMnO_x$-R3 (**Table 2**). However, the similar S_{BET} relative decrease of the two catalysts after PPC tests as compared to those obtained after catalysis tests does not allow to conclude on this point.

Figure 7 shows the CO, CO_2 and CO_x yields as a function of ED (60-120 J.L^{-1}) for the two catalysts ($CuMnO_x$-R3 and $CuMn_2O_4$-P4) in PPC configuration in comparison with the NTP alone configuration. The CO_x yield is significantly improved in PPC configuration when compared to NTP and CO_x yield increases with ED in PPC using $CuMn_2O_4$-P4 whereas it decreases using $CuMnO_x$-R3 (**Figure 7**).

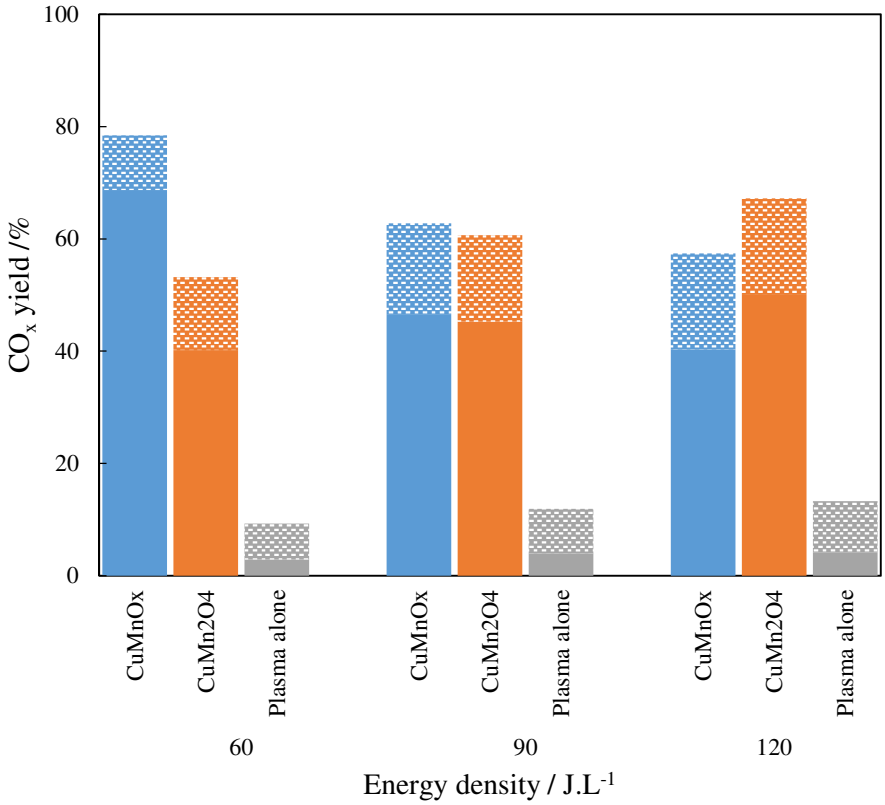

Figure 7. CO_x yield for NTP (ED = 60, 90 and 120 J.L^{-1}) and post-plasma catalysis (ED = 60, 90 and 120 J/L; catalyst temperature = 150°C) experiments (solid bars: CO_2 yield; hatched bars: CO yield)

Interestingly, when comparing to MnO_x and Ce-Mn oxides tested in the same pin-to-plate DC corona plasma reactor, except that the number of pins herein is increased from 5 to 10 [22], $CuMnO_x$-R3 and $CuMn_2O_4$-P4 exhibit better performances in terms of CO_2 yield. Indeed it has been reported, that in the presence of 1 g of MnO_y or $CeMn_x$ catalysts in PPC configuration (catalyst at 150°C ; RH = 10 %) the CO_2 yield reached the value of ~ 30 % for ED= 240 J.L^{-1}[22]. While using 2 times less energy (ED = 120 J.L^{-1}) and half the catalyst amount (0.5g), $CuMnO_x$-R3 and $CuMn_2O_4$-P4 led to CO_2 yield of ~ 50% evidencing the high performances of these catalysts in PPC configuration for TCE abatement.

Ye et al. underlined the importance of the decomposition of ozone on catalyst surface for a better performance in PPC process in their review work [52]. It is generally proposed that the ozone decomposition over transition metal leads to the formation of reactive oxygen species (O^- and/or O_2^{2-}). Concerning the PPC experiments the decomposition of ozone is quantitative showing the efficiency of the plasma assisted catalysts. However the $[O_3]/[TCE]_0$ ratios are far less from the stoichiometric one of 4 considering the total transformation of initial amount of C into CO_2 as follow :

$$C_2Cl_3H + 4\ O_3 = 2\ CO_2 + 4\ O_2 + HCl + Cl_2 \quad (5)$$

Therefore, the high production of CO_2 cannot be explained solely by the ability of the plasma assisted catalyst to decompose efficiently O_3. It is suggested that the plasma generated gaseous by-products (see below) also contribute to such an increase by a better activation of the catalyst at 150°C.

Figures 8 and **9** show the FT-IR spectra of the inlet TCE polluted humid air and of the outlet gaseous streams after plasma treatment (NTP alone at ED of 90 J.L^{-1}; PPC at ED of 60, 90, 120 J.L^{-1}) using

$CuMn_2O_4$-P4 and $CuMnO_x$-R3 (T_c = 150°C), respectively. The FT-IR spectrum of the inlet TCE shows the characteristic bands of TCE [36].

With NTP alone at 90 J.L^{-1}, the TCE decomposition is clearly observed by the decrease in intensity of the C-H out of plane deformation band at the wavelength of 945 cm^{-1}. Furthermore, it is found along the bands of TCE the characteristic bands of the plasma generated (oxi)chlorinated by-products such as dichloroacetylchloride (DCAC), trichloroacetaldehyde (TCAD) and phosgene (PG). The formation of TCAD is difficult to identify due to the presence of water absorption bands. The detection and possible reaction schemes of formation of such intermediate oxidation products have already been observed and discussed elsewhere [23,36]. Meanwhile, the formation of ozone is also detected from the bands at 1014-1046 cm^{-1} [53,54].

In PPC configuration at 60 J.L^{-1}, as compared with NTP alone at 90 J.L^{-1}, the intensity of the band at 945 cm^{-1} decreases to a higher extent while the intensity of the bands corresponding to CO_2 vibrations increases whatever the catalyst under concern. Similarly, the bands of ozone totally disappeared. This O_3 consumption can be related to the significant decrease of the DCAC and TCAD productions as observed by the decrease in intensity of the bands located at 1760 cm^{-1}, 1076 cm^{-1}, 1055 cm^{-1}, 989 cm^{-1} and 740 cm^{-1} and 1773 cm^{-1}, respectively. On the other hand, it is found that the increase of ED has not beneficial effect on the decrease of PG production when using $CuMn_2O_4$-P4 (**Figure 8**). By comparison the amount of PG is highly reduced over $CuMnO_x$-R3 at 60 J.L^{-1} (**Figure 9**). However, when increasing further ED, the production of PG slightly increases in line with a surface (oxi)chorination of the catalyst consistent with XPS data (see below).

Whatever the PPC configuration under investigation, it is noticeable that the emergence of new bands corresponding to C-Cl bond vibration relative to $CHCl_3$ and CCl_4 located at the wavenumber of 774 cm^{-1} and 794 cm^{-1}, respectively [21]. Such chlorinated C1 formations can be explained by the reaction of $CHCl_2$ and CCl_3 radicals resulting mainly from the easy cleavage of the carbon-carbon bond of DCAC with adsorbed chlorine [23]. Based on the ratio of C-Cl bond vibration intensity, the relative proportion of $CHCl_3$ seems to be higher over $CuMnO_x$-R3 despite the higher content of chlorine detected by XPS analysis.

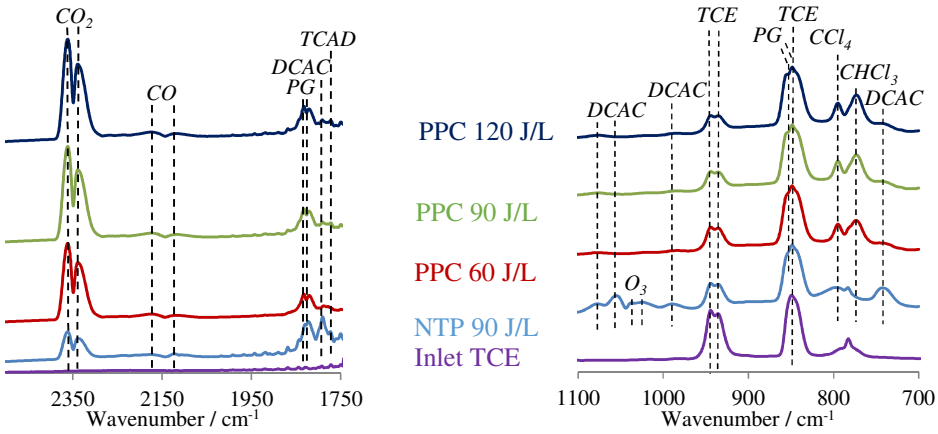

Figure 8. FT-IR spectra in the wavenumber range 2500-1750 cm^{-1} and 1100–700 cm^{-1} of inlet TCE polluted air stream and outlet stream after NTP and PPC process (Catalyst: $CuMn_2O_4$-P4; ED of PPC: 60-120 J.L^{-1}; ED of NTP: 90 J.L^{-1}; PG: phosgene, DCAC: dichloroacetylchloride and TCAD: trichloroacetaldehyde)

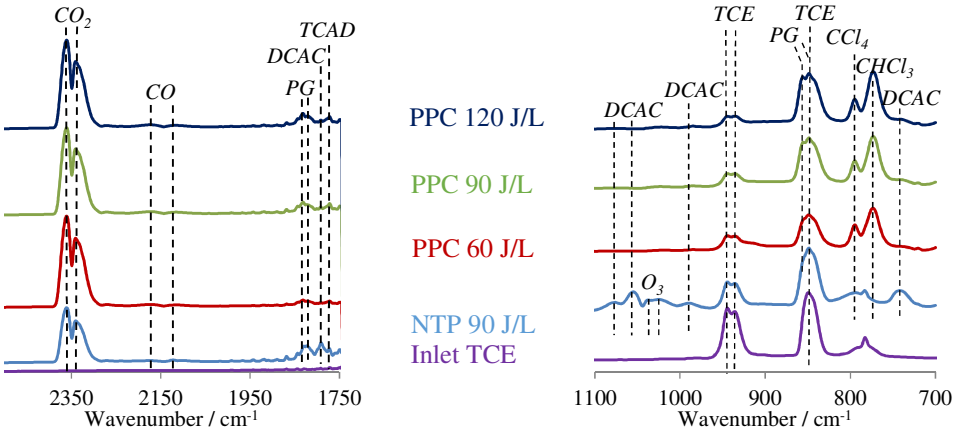

Figure 9. FT-IR spectra in the wavenumber range 2500-1750 cm^{-1} and 1100–700 cm^{-1} of inlet TCE polluted air stream and outlet stream after NTP and PPC process (Catalyst: $CuMnO_x$-R3; ED of PPC: 60-120 $J.L^{-1}$; ED of NTP: 90 $J.L^{-1}$; PG: phosgene, DCAC: dichloroacetylchloride and TCAD: trichloroacetaldehyde)

The elemental composition of the fresh and used (after PPC process) catalysts is given in **Table 2**. Taking into account the margin of error of the ICP analysis, Mn/Cu atomic ratio of both materials remained constant after PPC experiments. XPS results obtained from the fresh and used (catalysts after PPC experiments) are summarized in **Table 4**. The Cu 2p envelopes can be simulated considering that Cu 2p and Mn LMM_b Auger peaks overlaps [35]. For $CuMn_2O_4$-P4 catalyst, the Cu $2p_{3/2}$ envelope shows two distinct photopeaks at 931.2 and 934.0 eV whose values can be attributed to Cu^+ and Cu^{2+} species, respectively (**Figure 10**). Conversely, the $CuMnO_x$-R3 sample exhibits one single Cu $2p_{3/2}$ photopeak with BE of 934.3 eV attributed to the sole presence of Cu^{2+} species ((**Figure 10**). Both catalysts show a high XPS Mn AOS amounting to 3.7 and 3.5 for $CuMn_2O_4$-P4 and $CuMnO_x$-R3, respectively. In terms of Mn/Cu XPS ratios determined considering the presence of Mn LMM_b Auger component in the Cu 2p region, we obtained values of 3.7 and 5.1 for $CuMn_2O_4$-P4 and $CuMnO_x$-R3, respectively.

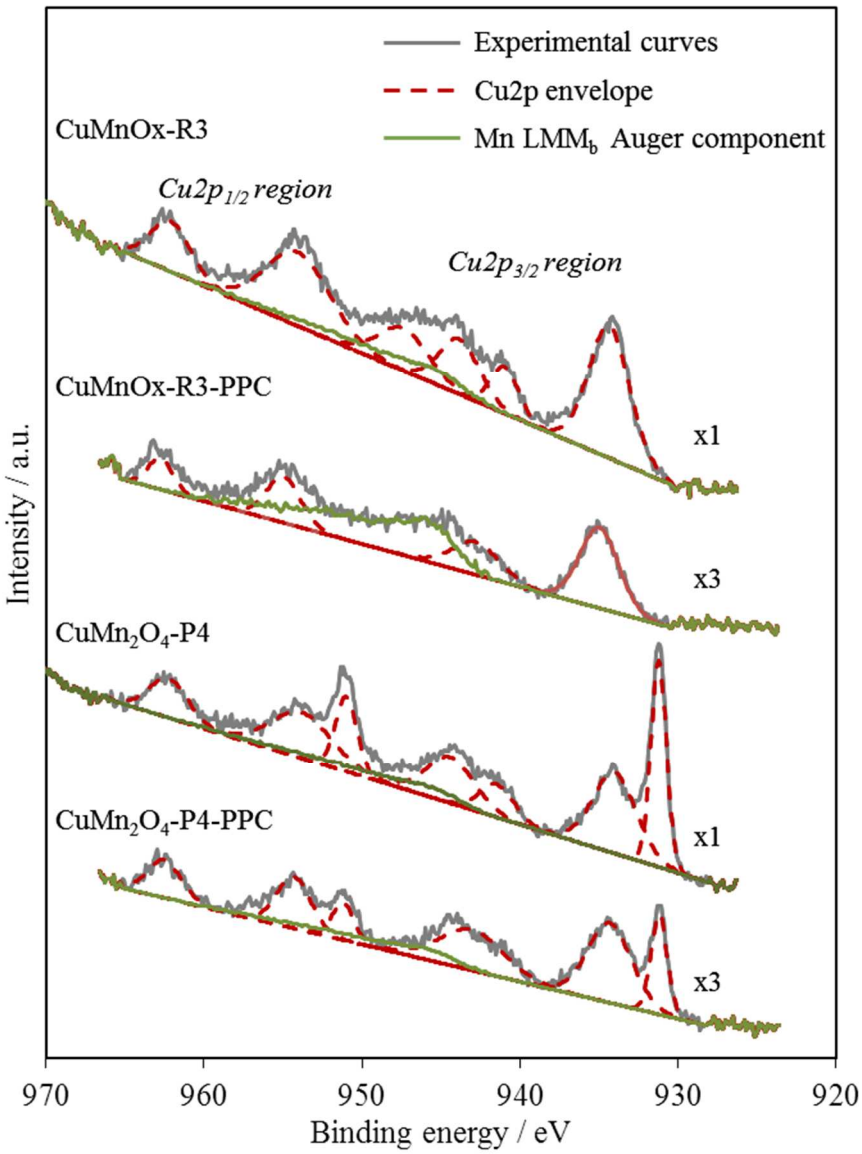

Figure 10. Simulated Cu 2p spectra obtained for $CuMn_2O_4$-P4 and $CuMnO_x$-R3 samples before and after PPC process

After PPC, it is found for $CuMn_2O_4$-P4 a decrease by one half of the Cu^+/Cu^{2+} atomic ratio accompanied with a concomitant Mn AOS decrease from 3.7 to 2.9 and a slight surface Cu enrichment (Mn/Cu = 2.9). For $CuMnO_x$-R3, a significant decrease of the XPS Mn AOS is noticed (3.5 to 2.9) and the atomic Mn/Cu ratio is also slightly decreased (4.5 compared to 5.1).

Table 4. XPS results on the fresh and used catalysts (after PPC tests)

Sample	Cu $2p_{3/2}$ BE (eV)	Mn AOS	Mn/Cu[a]	Cl/(Cu+Mn)[a]	Cu^{+}/Cu^{2+}
$CuMn_2O_4$-P4	931.2, 934.0	3.7	3.7	-	0.5
$CuMn_2O_4$-P4-PPC	931.1, 934.2	2.9	2.9	0.15	0.24
$CuMnO_x$-R3	934.3	3.5	5.1	-	0
$CuMnO_x$-R3-PPC	934.8	2.9	4.5	0.25	0

[a] atomic ratio

After PPC, chlorine element has been detected at the surface of both catalysts. Such chlorine detection can be explained by the incomplete TCE degradation during the PPC process. The Cl 2p envelopes can be simulated considering one type of chlorine (**Figure 11**). The Cl $2p_{3/2}$ and Cl $2p_{1/2}$ photopeaks were found at 198.7 and 200.3 eV for $CuMn_2O_4$-P4-PPC and 198.5 and 200.1 eV for $CuMnO_x$-R3-PPC, respectively. The location of Cl $2p_{3/2}$ photopeak BEs at 198.7/198.5 eV can be attributed to metal (M) (oxi)chloride, with M= Cu and/or Mn [14]. As a consequence, the presence of organic chloride species can be excluded on both the catalyst surfaces. This can be due to the beneficial effect of water enabling the efficient removal of chlorinated organic ad-species [20]. In addition, the XPS atomic Cl/(Cu + Mn) ratio is 0.15 for $CuMn_2O_4$-P4-PPC, whereas for $CuMnO_x$-R3-PPC, it increases up to 0.25 (**Table 4**). It is suggested that the differences in terms of surface area, Cu-Mn interactions and amorphous-crystalline structure may play a role in the different relative amount of chlorine detected on different catalysts.

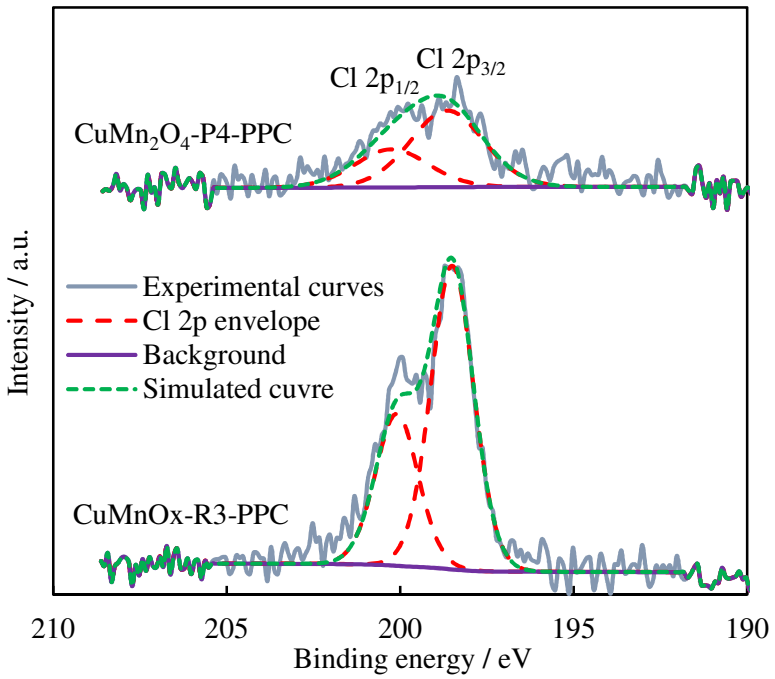

Figure 11. Cl 2p spectra obtained for $CuMn_2O_4$-P4 and $CuMnO_x$-R3 samples after PPC process

Based on these results, the extent of chlorination is more pronounced for $CuMnO_x$-R3. We speculate a surface transformation of the catalyst to give some (oxi)choride Mn(Cu) phases less active than the starting catalyst phase which can explain that the TCE conversion does not increase with ED. By

opposition, it is postulated that the presence of a crystallized spinel $CuMn_2O_4$ having two redox couples Cu^{2+}/Cu^{+} and Mn^{4+}/Mn^{3+} leads to a more stable catalyst towards chlorination.

4. Conclusion

The preparation method of the Cu-Mn oxide catalysts has a significant influence on its performance in PPC removal of dilute TCE at 150°C. The better results are obtained with the plasma assisted Cu-Mn oxide prepared by redox method working at 150 °C enabling to achieve more than 80% TCE conversion with a CO_x yield of 78% for the lowest investigated ED (60 $J.L^{-1}$). In this configuration the formation of gaseous chlorinated by-products is minimized but not totally suppressed. This can be explained in part by the low plasma generated O_3 production which does not allow to supply enough active oxygen allowing total decomposition of the plasma generated hazardous compounds. Besides the high CO_2 production might be also explained by the beneficial role of plasma generated gaseous by-products contributing to a better activation of the catalyst at 150°C. Although, Cu-Mn oxide prepared by co-precipitation method showed a lower TCE conversion, it exhibited a better stability in the PPC process for TCE abatement.

Acknowledgements

The joint research program PICS n°6913 (Preparation of catalysts and catalytic depollution assisted by plasma) from CNRS, the "DepollutAir" project (grant number 1.1.18) of the European Program INTERREG V France-Wallonie-Flanders (FEDER), Chevreul institute (FR 2638), Ministère de l'Enseignement Supérieur et de la Recherche and Région Hauts-de-France are acknowledged for the funding and their support for this work.

References

[1] M. Kampa, E. Castanas, Human health effects of air pollution, Environ. Pollut. 151 (2008) 362–367. doi:10.1016/j.envpol.2007.06.012.

[2] K. Nikolajsen, L. Kiwi-Minsker, A. Renken, Structured fixed-bed adsorber based on zeolite/sintered metal fibre for low concentration VOC removal, Chem. Eng. Res. Des. 84 (2006) 562–568. doi:10.1205/cherd.05220.

[3] Z. Zhang, Z. Jiang, W. Shangguan, Low-temperature catalysis for VOCs removal in technology and application: A state-of-the-art review, Catal. Today. 264 (2016) 270–278. doi:10.1016/j.cattod.2015.10.040.

[4] M.S. Kamal, S.A. Razzak, M.M. Hossain, Catalytic oxidation of volatile organic compounds (VOCs)-A review, Atmos. Environ. 140 (2016) 117–134. doi:10.1016/j.atmosenv.2016.05.031.

[5] A. Kumar, J. Dewulf, H. Van Langenhove, Membrane-based biological waste gas treatment, Chem. Eng. J. 136 (2008) 82–91. doi:10.1016/j.cej.2007.06.006.

[6] C. Subrahmanyam, A. Renken, L. Kiwi-Minsker, Catalytic non-thermal plasma reactor for abatement of toluene, Chem. Eng. J. 160 (2010) 677–682. doi:10.1016/j.cej.2010.04.011.

[7] W. Liang, J. Li, J. Li, Y. Jin, Abatement of toluene from gas streams via ferro-electric packed bed dielectric barrier discharge plasma, J. Hazard. Mater. 170 (2009) 633–638.

doi:10.1016/j.jhazmat.2009.05.019.

[8] T. Yamamoto, K. Ramanathan, P.A. Lawless, D.S. Ensor, J.R. Newsome, N. Plaks, G.. Ramsey, Control of volatile organic compounds by an ac energized ferroelectric pellet reactor and a pulsed corona reactor, IEEE Trans. Ind. Appl. 28 (1992) 528–534. doi:10.1109/IAS.1989.96941.

[9] F. Holzer, F.D. Kopinke, U. Roland, Influence of ferroelectric materials and catalysts on the performance of non-thermal plasma (NTP) for the removal of air pollutants, Plasma Chem. Plasma Process. 25 (2005) 595–611. doi:10.1007/s11090-005-6804-1.

[10] M. Schiavon, V. Torretta, A. Casazza, M. Ragazzi, Non-thermal plasma as an innovative option for the abatement of volatile organic compounds: a review, Water, Air, Soil Pollut. 228 (2017) 388. doi:10.1007/s11270-017-3574-3.

[11] F. Thevenet, L. Sivachandiran, O. Guaitella, C. Barakat, A. Rousseau, Plasma-catalyst coupling for volatile organic compound removal and indoor air treatment: a review, J. Phys. D. Appl. Phys. 47 (2014) 1–14. doi:10.1088/0022-3727/47/22/224011.

[12] H.L. Chen, H.M. Lee, S.H. Chen, M.B. Chang, S.J. Yu, S.N. Li, Removal of volatile organic compounds by single-stage and two-stage plasma catalysis systems: a review of the performance enhancement mechanisms, current status, and suitable applications, Environ. Sci. Technol. 43 (2009) 2216–2227. doi:10.1021/es802679b.

[13] K. Abedi, F. Ghorbani-Shahna, B. Jaleh, A. Bahrami, R. Yarahmadi, R. Haddadi, M. Gandomi, Decomposition of chlorinated volatile organic compounds (CVOCs) using NTP coupled with TiO_2/GAC, ZnO/GAC, and TiO_2–ZnO/GAC in a plasma-assisted catalysis system, J. Electrostat. 73 (2015) 80–88. doi:10.1016/j.elstat.2014.10.008.

[14] A.M. Vandenbroucke, M.T. Nguyen Dinh, N. Nuns, J.-M. Giraudon, N. De Geyter, C. Leys, J.-F. Lamonier, R. Morent, Combination of non-thermal plasma and Pd/$LaMnO_3$ for dilute trichloroethylene abatement, Chem. Eng. J. 283 (2016) 668–675. doi:10.1016/J.cej.2015.07.089.

[15] X. Tu, H.J. Gallon, J.C. Whitehead, Electrical and spectroscopic diagnostics of a single-stage plasma-catalysis system: effect of packing with TiO_2, J. Phys. D. Appl. Phys. 44 (2011) 1–4. doi:10.1088/0022-3727/44/48/482003.

[16] J. Wu, Q. Xia, H. Wang, Z. Li, Catalytic performance of plasma catalysis system with nickel oxide catalysts on different supports for toluene removal: Effect of water vapor, Appl. Catal. B Environ. 156–157 (2014) 265–272. doi:10.1016/j.apcatb.2014.03.017.

[17] S. Kaliya Perumal Veerapandian, C. Leys, N. De Geyter, R. Morent, Abatement of VOCs using packed bed non-thermal plasma reactors: A review, Catalysts. 7 (2017) 1–34. doi:10.3390/catal7040113.

[18] T. Oda, T. Takahashi, K. Yamaji, TCE decomposition by the nonthermal plasma process concerning ozone effect, IEEE Trans. Ind. Appl. 40 (2004) 1249–1256. doi:10.1109/tia.2004.834068.

[19] A.M. Vandenbroucke, M. Mora, C. Jiménez-Sanchidrián, F.J. Romero-Salguero, N. De Geyter, C. Leys, R. Morent, TCE abatement with a plasma-catalytic combined system using MnO_2 as catalyst, Appl. Catal. B Environ. 156–157 (2014) 94–100. doi:10.1016/J.APCATB.2014.03.007.

[20] N. Nuns, A. Beaurain, M.T. Nguyen Dinh, A. Vandenbroucke, N. De Geyter, R.

Morent, C. Leys, J.-M. Giraudon, J.-F. Lamonier, A combined ToF-SIMS and XPS study for the elucidation of the role of water in the performances of a Post-Plasma Process using $LaMnO_{3+\delta}$ as catalyst in the total oxidation of trichloroethylene, Appl. Surf. Sci. 320 (2014) 154–160. doi:10.1016/j.apsusc.2014.09.047.

[21] M.T. Nguyen Dinh, J.-M. Giraudon, J.-F. Lamonier, A. Vandenbroucke, N. De Geyter, C. Leys, R. Morent, Plasma-catalysis of low TCE concentration in air using $LaMnO_{3+\delta}$ as catalyst, Appl. Catal. B Environ. 147 (2014) 904–911. doi:10.1016/j.apcatb.2013.07.008.

[22] M.T. Nguyen Dinh, J.-M. Giraudon, A.M. Vandenbroucke, R. Morent, N. De Geyter, J.-F. Lamonier, Post plasma-catalysis for total oxidation of trichloroethylene over Ce–Mn based oxides synthesized by a modified "redox-precipitation route," Appl. Catal. B Environ. 172–173 (2015) 65–72. doi:10.1016/j.apcatb.2015.02.013.

[23] M.T. Nguyen Dinh, J.-M. Giraudon, A.M. Vandenbroucke, R. Morent, N. De Geyter, J.-F. Lamonier, Manganese oxide octahedral molecular sieve K-OMS-2 as catalyst in post plasma-catalysis for trichloroethylene degradation in humid air, J. Hazard. Mater. 314 (2016) 88–94. doi:10.1016/j.jhazmat.2016.04.027.

[24] S. Sultana, Z. Ye, S. Kaliya Perumal Veerapandian, A. Löfberg, N. De Geyter, R. Morent, J.-M. Giraudon, J.-F. Lamonier, Synthesis and catalytic performances of K-OMS-2, Fe/K-OMS-2 and Fe-K-OMS-2 in post plasma-catalysis for dilute TCE abatement, Catal. Today. 307 (2018) 20–28. doi:10.1016/j.cattod.2017.05.078.

[25] A.M. Vandenbroucke, R. Aerts, W. Van Gaens, N. De Geyter, C. Leys, R. Morent, A. Bogaerts, Modeling and experimental study of trichloroethylene abatement with a negative direct current corona discharge, Plasma Chem. Plasma Process. 35 (2015) 217–230. doi:10.1007/s11090-014-9584-7.

[26] A.B. Lamb, W.C. Bray, J.C.W. Frazer, The removal of carbon monoxide from air, J. Ind. Eng. Chem. 12 (1920) 213–221. doi:10.1021/ie50123a007.

[27] T. Biemelt, K. Wegner, J. Teichert, M.R. Lohe, J. Martin, J. Grothe, S. Kaskel, Hopcalite nanoparticle catalysts with high water vapour stability for catalytic oxidation of carbon monoxide, Appl. Catal. B Environ. 184 (2016) 208–215. doi:10.1016/j.apcatb.2015.11.008.

[28] M. Krämer, T. Schmidt, K. Stöwe, W.F. Maier, Structural and catalytic aspects of sol–gel derived copper manganese oxides as low-temperature CO oxidation catalyst, Appl. Catal. A Gen. 302 (2006) 257–263. doi:10.1016/j.apcata.2006.01.018.

[29] A. Marinoiu, M. Raceanu, C. Cobzaru, C. Teodorescu, D. Marinescu, A. Soare, M. Varlam, Low temperature CO retention using hopcalite catalyst for fuel cell applications, React. Kinet. Mech. Catal. 112 (2014) 37–50. doi:10.1007/s11144-014-0694-2.

[30] V.H. Vu, J. Belkouch, A. Ould-Dris, B. Taouk, Removal of hazardous chlorinated VOCs over Mn-Cu mixed oxide based catalyst, J. Hazard. Mater. 169 (2009) 758–765. doi:10.1016/j.jhazmat.2009.04.010.

[31] H. Einaga, A. Kiya, S. Yoshioka, Y. Teraoka, G.J. Hutchings, N. Maguire, S.O. Shekhtman, S.H. Taylor, C. Lamberti, Catalytic properties of copper–manganese mixed oxides prepared by coprecipitation using tetramethylammonium hydroxide, Catal. Sci. Technol. 4 (2014) 3713–3722. doi:10.1039/C4CY00660G.

[32] E.C. Njagi, C.-H. Chen, H. Genuino, H. Galindo, H. Huang, S.L. Suib, Total oxidation of CO at ambient temperature using copper manganese oxide catalysts prepared by a redox method, Appl. Catal. B Environ. 99 (2010) 103–110. doi:10.1016/j.apcatb.2010.06.006.

[33] L. Matějová, P. Topka, K. Jirátová, O. Šolcová, Total oxidation of model volatile organic compounds over some commercial catalysts, Appl. Catal. A Gen. 443–444 (2012) 40–49. doi:10.1016/J.APCATA.2012.07.018.

[34] Y. Gu, Y. Yang, Y. Qiu, K. Sun, X. Xu, Combustion of dichloromethane using copper–manganese oxides supported on zirconium modified titanium-aluminum catalysts, Catal. Commun. 12 (2010) 277–281. doi:10.1016/J.CATCOM.2010.10.006.

[35] Z. Ye, J.-M. Giraudon, N. Nuns, P. Simon, N. De Geyter, R. Morent, J.-F. Lamonier, Influence of the preparation method on the activity of copper-manganese oxides for toluene total oxidation, Appl. Catal. B Environ. 223 (2018) 154–166. doi:10.1016/j.apcatb.2017.06.072.

[36] A.M. Vandenbroucke, M.T. Nguyen Dinh, J.-M. Giraudon, R. Morent, N. De Geyter, J.-F. Lamonier, C. Leys, Qualitative by-product identification of plasma-assisted TCE abatement by mass spectrometry and fourier-transform infrared spectroscopy, Plasma Chem. Plasma Process. 31 (2011) 707–718. doi:10.1007/s11090-011-9310-7.

[37] Y.S. Akishev, A.A. Deryugin, I. V. Kochetov, A.P. Napartovich, N.I. Trushkin, Dc glow discharge in air flow at atmospheric pressure in connection with waste gases treatment, J. Phys. D. Appl. Phys. 26 (1993) 1630–1637. doi:10.1088/0022-3727/26/10/014.

[38] Y.S. Akishev, M.E. Grushin, I. V. Kochetov, a. P. Napartovich, M. V. Pan'kin, N.I. Trushkin, Transition of a multipin negative corona in atmospheric air to a glow discharge, Plasma Phys. Reports. 26 (2000) 157–163. doi:10.1134/1.952826.

[39] U. Kogelschatz, Dielectric-barrier discharges: Their history, discharge physics, and industrial applications, Plasma Chem. Plasma Process. 23 (2003) 1–46. doi:10.1023/A:1022470901385.

[40] S. Pekárek, Non-thermal plasma ozone generation, Acta Polytech. 43 (2003) 47–51.

[41] O. Bertrand, G. Weber, S. Maure, V. Bernardet, J.P. Bellat, C. Paulin, Spectroscopic signatures of VOC physisorption on microporous solids. Application for trichloroethylene and tetrachloroethylene adsorption on MFI zeolites, J. Phys. Chem. B. 109 (2005) 13312–13321. doi:10.1021/jp048442a.

[42] H. Li, G. Lu, Q. Dai, Y. Wang, Y. Guo, Y. Guo, Efficient low-temperature catalytic combustion of trichloroethylene over flower-like mesoporous Mn-doped CeO_2 microspheres, Appl. Catal. B Environ. 102 (2011) 475–483. doi:10.1016/j.apcatb.2010.12.029.

[43] N. Blanch-Raga, A.E. Palomares, J. Martínez-Triguero, M. Puche, G. Fetter, P. Bosch, The oxidation of trichloroethylene over different mixed oxides derived from hydrotalcites, Appl. Catal. B Environ. 160–161 (2014) 129–134. doi:10.1016/j.apcatb.2014.05.014.

[44] R. López-Fonseca, J.I. Gutiérrez-Ortiz, M.A. Gutiérrez-Ortiz, J.R. González-Velasco, Dealuminated Y zeolites for destruction of chlorinated volatile organic compounds, J.

Catal. 209 (2002) 145–150. doi:10.1006/jcat.2002.3591.

[45] M. Romero-Sáez, D. Divakar, A. Aranzabal, J.R. González-Velasco, J.A. González-Marcos, Catalytic oxidation of trichloroethylene over Fe-ZSM-5: Influence of the preparation method on the iron species and the catalytic behavior, Appl. Catal. B Environ. 180 (2016) 210–218. doi:10.1016/j.apcatb.2015.06.027.

[46] N. Blanch-Raga, A.E. Palomares, J. Martínez-Triguero, S. Valencia, Cu and Co modified beta zeolite catalysts for the trichloroethylene oxidation, Appl. Catal. B Environ. 187 (2016) 90–97. doi:10.1016/j.apcatb.2016.01.029.

[47] D. Divakar, M. Romero-Sáez, B. Pereda-Ayo, A. Aranzabal, J.A. González-Marcos, J.R. González-Velasco, Catalytic oxidation of trichloroethylene over Fe-zeolites, Catal. Today. 176 (2011) 357–360. doi:10.1016/j.cattod.2010.11.065.

[48] J.R. González-Velasco, A. Aranzabal, J.I. Gutiérrez-Ortiz, R. López-Fonseca, M.A. Gutiérrez-Ortiz, Activity and product distribution of alumina supported platinum and palladium catalysts in the gas-phase oxidative decomposition of chlorinated hydrocarbons, Appl. Catal. B Environ. 19 (1998) 189–197. doi:10.1016/S0926-3373(98)00078-2.

[49] D.C. Kim, S.-K. Ihm, Application of spinel-type cobalt chromite as a novel catalyst for combustion of chlorinated organic pollutants, Environ. Sci. Technol. 35 (2001) 222–226. doi:10.1021/es001098k.

[50] J. Corella, J.M. Toledo, A.M. Padilla, On the selection of the catalyst among the commercial platinum-based ones for total oxidation of some chlorinated hydrocarbons, Appl. Catal. B Environ. 27 (2000) 243–256. doi:10.1016/S0926-3373(00)00154-5.

[51] B. Mendyka, A. Musialik-Piotrowska, K. Syczewska, Effect of chlorine compounds on the deactivation of platinum catalysts, Catal. Today. 11 (1992) 597–610. doi:10.1016/0920-5861(92)80044-N.

[52] Z. Ye, J.-M. Giraudon, N. De Geyter, R. Morent, J.-F. Lamonier, The design of MnO_x based catalyst in post-plasma catalysis configuration for toluene abatement, Catalysts. 8 (2018) 1–32. doi:10.3390/catal8020091.

[53] R. Morent, C. Leys, Ozone generation in air by a DC-excited multi-pin-to-plane plasma source, Ozone Sci. Eng. 27 (2005) 239–245. doi:10.1080/01919510590945813.

[54] B. Eliasson, M. Hirth, U. Kogelschatz, Ozone synthesis from oxygen in dielectric barrier discharges, J. Phys. D. Appl. Phys. 20 (1987) 1421–1437. doi:10.1088/0022-3727/20/11/010.

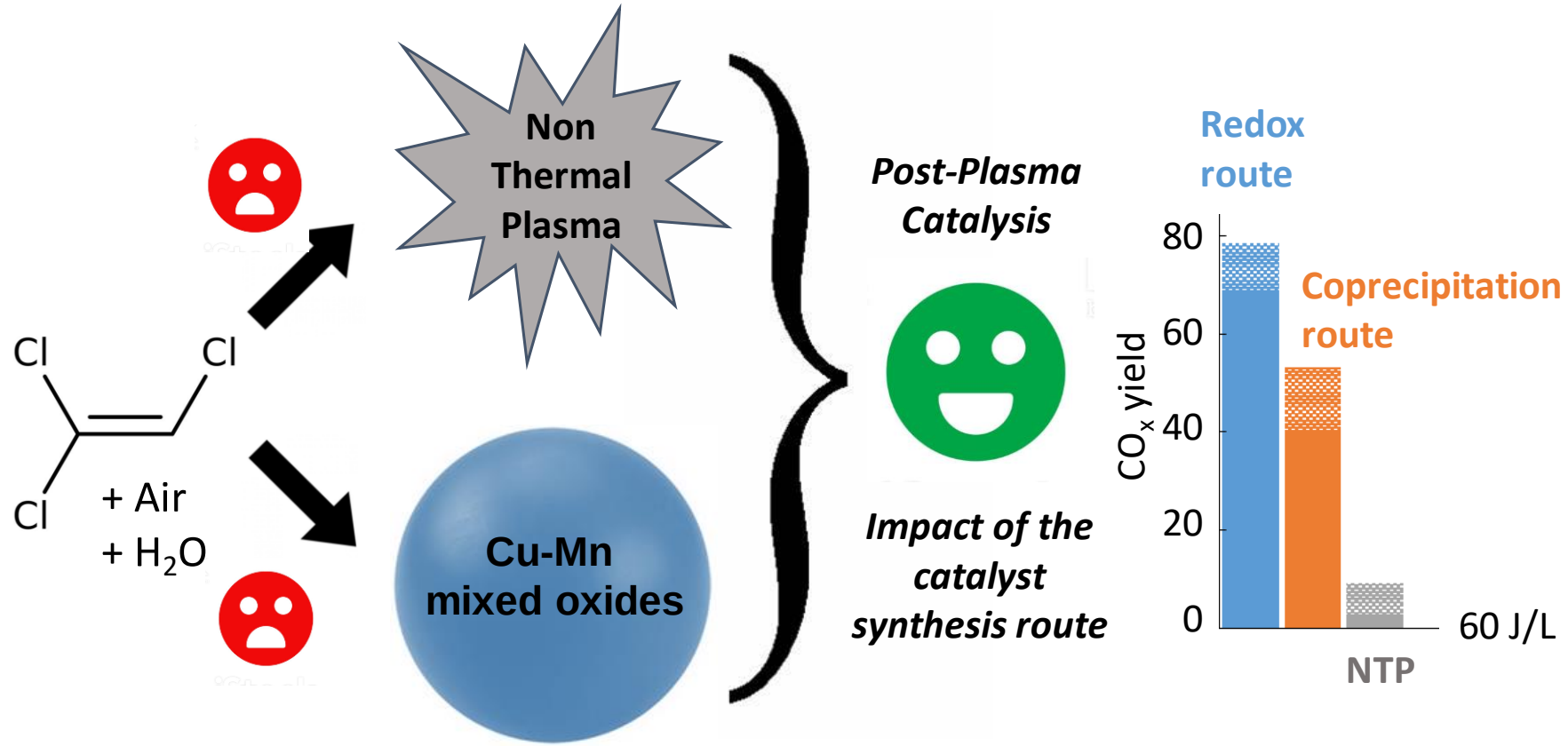
Cl
Cl
Cl
+ Air
+ H_2O
Non Thermal Plasma
Cu-Mn mixed oxides
Post-Plasma Catalysis
Impact of the catalyst synthesis route
Redox route
Coprecipitation route
CO_x yield
80
60
40
20
0
60 J/L
NTP